Microfluidic platform for characterizing TCR–pMHC interactions

Citation: Stockslager, Max A., Josephine Shaw Bagnall, Vivian C. Hecht, Kevin Hu, Edgar Aranda-Michel, Kristofor Payer, Robert J. Kimmerling, and Scott R. Manalis. "Microfluidic Platform for Characterizing TCR–pMHC Interactions." Biomicrofluidics 11, no. 6 (November 2017): 064103.

As Published: http://dx.doi.org/10.1063/1.5002116

Publisher: AIP Publishing

Persistent URL: http://hdl.handle.net/1721.1/119858

Version: Final published version: final published article, as it appeared in a journal, conference proceedings, or other formally published context

Microfluidic platform for characterizing TCR–pMHC interactions

Max A. Stockslager,[1,a)] Josephine Shaw Bagnall,[2,a)] Vivian C. Hecht,[2,a)] Kevin Hu,[2] Edgar Aranda-Michel,[2] Kristofor Payer,[3] Robert J. Kimmerling,[2] and Scott R. Manalis[1,2,4]

[1]*Department of Mechanical Engineering, Massachusetts Institute of Technology, Cambridge, Massachusetts 02139, USA*
[2]*Department of Biological Engineering, Massachusetts Institute of Technology, Cambridge, Massachusetts 02139, USA*
[3]*Microsystems Technology Laboratories, Massachusetts Institute of Technology, Cambridge, Massachusetts 02139, USA*
[4]*Koch Institute for Integrative Cancer Research, Massachusetts Institute of Technology, Cambridge, Massachusetts 02139, USA*

(Received 29 August 2017; accepted 20 October 2017; published online 14 November 2017)

The physical characteristics of the T cell receptor (TCR)–peptide-major histocompatibility complex (pMHC) interaction are known to play a central role in determining T cell function in the initial stages of the adaptive immune response. State-of-the-art assays can probe the kinetics of this interaction with single-molecular-bond resolution, but this precision typically comes at the cost of low throughput, since the complexity of these measurements largely precludes "scaling up." Here, we explore the feasibility of detecting specific TCR–pMHC interactions by flowing T cells past immobilized pMHC and measuring the reduction in cell speed due to the mechanical force of the receptor-ligand interaction. To test this new fluidic measurement modality, we fabricated a microfluidic device in which pMHC-coated beads are immobilized in hydrodynamic traps along the length of a serpentine channel. As T cells flow past the immobilized beads, their change in speed is tracked via microscopy. We validated this approach using two model systems: primary $CD8^+$ T cells from an OT-1 TCR transgenic mouse with beads conjugated with H-$2K^b$:SIINFEKL, and Jurkat T cells with beads conjugated with anti-CD3 and anti-CD28 antibodies. *Published by AIP Publishing.* https://doi.org/10.1063/1.5002116

I. INTRODUCTION

The kinetic,[1–3] mechanical,[4] and thermodynamic[5] characteristics of the interactions between T cell receptors (TCRs) and peptide-major histocompatibility complexes (pMHCs) play a central role in determining T cell function in the initiation of the adaptive immune response. In particular, the affinity of TCR–pMHC binding (the ratio of the kinetic on-rate and off-rate) has been shown to correlate with T cell proliferation[6] and $CD8^+$ T cell lysis capacity[3] in various model systems.

A wide variety of techniques have been used to measure the specificity and affinity of the TCR–pMHC interaction, including surface plasmon resonance (SPR), micropipette aspiration, biomembrane force probes, Förster resonance energy transfer (FRET), and optical tweezers.[7] Most techniques involve two steps: inducing controlled TCR–pMHC interactions (either using T cells or isolated TCR) and transducing the resulting binding events into a detectable signal.

Each of these techniques is suited to different applications. Different measurement modalities can be compared based on their throughput (number of conditions measured per unit time) and their resolution (ability to distinguish different levels of affinity). Fundamentally, there

[a)]M. A. Stockslager, J. S. Bagnall, and Vivian C. Hecht contributed equally to this work.

exists a tradeoff between these two goals, that is, improvements in the resolution of affinity measurements generally come at the cost of reduced throughput, and vice versa. For example, pMHC tetramer staining enables high-throughput quantification of the numbers of antigen-specific T cells within a population, but lacks the resolution to distinguish between different levels of TCR affinity.

There has been a steady improvement in the achievable resolution of affinity measurements, with the most sensitive measurements enabling the probing of single molecular bonds.[8] This has enabled new insights; for example, high precision measurements by Liu *et al*. using micropipette aspiration-based techniques have revealed the force-dependence of single TCR–pMHC interactions for inducing T cell signaling.[9]

However, relatively little progress has been made toward increasing the throughput of these measurements—and in some applications, higher throughput would be more valuable than further improvements in affinity resolution. For example, adoptive T cell immunotherapy has emerged as a promising approach to cancer treatment in which tumor-specific $CD8^+$ T cells are isolated, expanded, and/or activated *ex vivo*, then re-infused to the patient to induce a more effective anti-tumor response. Evidence in mice[10,11] and in humans[12] suggests that affinity correlates with anti-tumor function in adoptive immunotherapy, and selecting donor T cells based on affinity has been shown to improve clinical outcomes in melanoma patients.[13] Therefore, these studies would benefit from a method for rapidly comparing the affinities of tens to hundreds or thousands of TCR sequences, in order to select the one with the greatest affinity for a specific peptide.

One possible route to increased throughput would be to parallelize the existing assays. However, these assays have proven difficult to scale up for a variety of reasons. For example, SPR is limited by the requirement to isolate the TCR and pMHC of interest and produce them in recombinant form, which is an expensive and laborious process. Other techniques such as micropipette aspiration and the biomembrane force probe have also been difficult to parallelize due to the requirement to precisely manipulate single cells.

We wondered whether a simpler, more scalable approach could be used to estimate the affinity of TCR–pMHC interactions without the requirement to manipulate individual cells. One possibility is to exploit the mechanical force associated with the TCR–pMHC bond by inducing interactions between flowing T cells and immobilized pMHC while measuring the change in cell speed that occurs as a result of the interaction. Using this fluidic measurement modality, the readout would be based on the net effect of many TCR–pMHC interactions rather than on the formation and rupture of single molecular bonds.

To determine whether this strategy could detect specific TCR–pMHC interactions, we fabricated microfluidic devices containing long serpentine channels, along which pMHC-coated beads are immobilized in hydrodynamic traps (Fig. 1). As T cells flow along the serpentine channel, their speeds are tracked continuously using optical microscopy. Using this approach, the reduction in cell speed when cells flow past pMHC-coated beads is then taken as a relative measure of TCR–pMHC affinity.

We tested whether this fluidic measurement modality could detect specific binding events in two model systems: Jurkat cells (a human-derived T lymphocyte cell line[14]) and primary murine $CD8^+$ T cells from an OT-1 TCR transgenic mice.[15]

II. RESULTS

A. Device design and operation

1. Interaction forces

Before fabricating the devices, we made scaling estimates to assess the feasibility of this measurement modality for detecting specific TCR–pMHC interactions. In order to detect speed changes resulting from cell-bead interactions, the magnitude of the cell-bead interaction force should be comparable to the viscous force experienced by the cell as it moves through the channel.

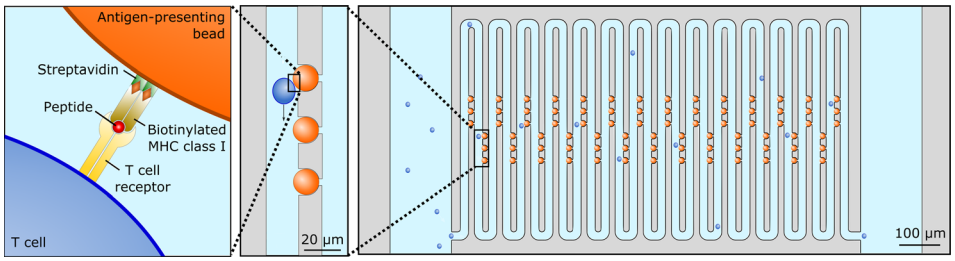

FIG. 1. Microfluidic trap array platform. As T cells flow through the serpentine channel, they come into contact with trapped antigen-presenting beads, resulting in TCR–pMHC interactions. Multiple TCR–pMHC may occur between a cell and a bead, although only one is shown for simplicity. These interactions decrease cell speed, which is tracked via optical microscopy.

At low Reynolds number (here, $Re < 10^{-3}$), the viscous force on the moving cell scales as μVD, where μ is the medium viscosity, V is a characteristic velocity, and D is the cell diameter. More precise force estimates can be made using more detailed descriptions of the flow; for example, using a published result for the correction to Stokes drag for a particle flowing in a confined channel,[16] we estimate that the viscous force on cells in the hydrodynamic trap array is approximately 100–200 pN. Cell-bead interaction forces much smaller than this value do not appreciably change cells' speeds as they flow past the immobilized beads, so no interaction is detectable; however, much larger interaction forces result in permanent attachment of cells to beads, since the interaction force dominates the forces driving the cell forward.

Estimating the cell-bead interaction force requires estimates of the force of each individual TCR:pMHC interaction as well as the number of bonds formed. The force of a single TCR-pMHC interaction is 1–10 pN,[9] and based on the spatial density of TCR and pMHC on the cells and beads used in this work, up to approximately 100 parallel interactions may form per cell-bead contact, for a total interaction force estimate $F_{\text{int}} \sim 100$–1000 pN. This value is comparable to the viscous force experienced by the cell, suggesting that the fluidic measurement modality is suitable for detecting TCR-pMHC interactions. On the other hand, antibody-antigen interactions are an order of magnitude stronger (10–100 pN per interaction, for a total force of 10^3–10^4 pN per cell-bead contact[17]), and therefore, we expect that these interactions should result in permanent attachment of cells to antibody-coated beads.

2. Hydrodynamic traps

We designed and fabricated an array of hydrodynamic traps that passively capture the pMHC-coated beads due to the difference in fluidic resistance across each trap versus along each turn of the serpentine channel.[18] Beads enter unoccupied traps due to their low fluidic resistance, but pass by occupied traps due to their increased resistance. Beads remain trapped as long as a small positive pressure difference is maintained across the array, allowing buffer exchange and loading of cell samples without bead loss.

A key parameter in designing effective hydrodynamic traps is the fraction of the serpentine channel's total volumetric flow rate that enters each unoccupied trap. This ratio is a function of the trap and serpentine channel dimensions. A commonly cited design rule is that the trap and channel geometry should be designed such that this fraction is greater than 50% to achieve acceptable trapping efficiency.[18,19] This fraction is highly sensitive to the channel and trap geometry. We used numerical simulations to estimate the flow rate fraction for a variety of channel designs and bead loading conditions. Details of the numerical simulations are included in Sec. IV.

In our most commonly used device design, the trap cups have diameter 15 μm, and the trap through-holes have 4 μm width and 2.3 μm length. The serpentine channel is 18 μm wide and 17 μm deep, and each of its 27 turns contains three traps. The simulated flow rate fractions for this design are 27%, 29%, and 34% for the first, second, and third traps, respectively.

Interestingly, we found that near 100% trapping efficiency is achieved even though these flow rate fractions are well below the commonly cited threshold of 50%.

Other design considerations include the number of traps placed along each lane of the serpentine channel and the radius of the trap "cup." Increasing the number of traps per lane increases the number of cell-bead interactions observed per cell. However, as more traps are added, the flow rate decreases at the downstream end of the lane, since each trap diverts some of the incoming fluid into the next lane. This can result in practical issues when operating the device, particularly when there are unoccupied traps. For example, since flow rates decrease dramatically around the bends of the serpentine channel, clearing the beads or cells from the channel becomes more difficult. In practice, we found that arrays with three traps per lane were ideal for maximizing the number of cell-bead interactions observed per cell while maintaining flow stability in the serpentine channel.

The arrays of traps are flanked by two large bypass channels with width 150 μm. The upstream and downstream pressures in each bypass are controlled independently by two electronic pressure regulators. This design decouples flow in the bypasses from flow across the hydrodynamic trap array, allowing introduction of different rinsing buffers or cell samples into the device while maintaining only a small, gentle pressure difference across the array to maintain the beads in the hydrodynamic traps.

3. Measuring cell-bead interactions on-chip

Videos of the hydrodynamic trap array are analyzed using MATLAB to track the trajectories and velocities of individual cells as they transit the serpentine channel. To validate the cell-tracking approach, we solved numerically for the velocity field in the trap array to compare to our experimental data [Fig. 2(a)]. Simulations indicated that even when all traps are occupied by inert 15 μm beads, cells are expected to accelerate and decelerate as they transit the serpentine channel. This effect occurs because the gaps are not fully occluded even when they are occupied by beads; approximately 14%, 12%, and 7% of the incoming volumetric flow rate is diverted through the first, second, and third traps, respectively, while the remaining 67% continues around the end of the serpentine channel [Fig. 2(b)]. Good qualitative agreement was observed between the numerical simulations of the velocity field and representative experimental data, in which Jurkat T cells were flowed past traps occupied by inert polystyrene beads [Fig. 2(c)].

To quantify these cell-bead interactions, we measure the extent to which each cell decelerates after it comes into contact with the beads. To this end, we divide the serpentine channel into "trap regions" and "non-trap regions" [Fig. 2(d)], representing the regions of the channel in which cells are or are not in contact with beads, respectively. We compute each cell's median speed as it passes through the trap regions, and normalize to the same cell's median speed as it passes through the non-trap regions. The resulting "speed ratio" quantifies the extent to which cells slow down after contacting beads. Since flow rates are faster in trap regions during normal operation, we expect the speed ratio to be greater than 1 if there is no cell-bead interaction. Cell-bead interaction forces tend to decrease the speed ratio, but depending on the strength of the interaction, the ratio may or may not be reduced below 1.

B. System characterization

1. Antibody-antigen interaction

We first asked whether this fluidic measurement modality could detect the relatively strong interactions between Jurkat T cells and carboxylated beads conjugated with anti-human CD3 and anti-human CD28 antibodies, which bind the TCR component CD3 and the coreceptor CD28 with forces 10–100 times greater than those of typical TCR–pMHC interactions. As a negative control, we loaded the trap array with inert polystyrene beads and recorded the interactions of Jurkat cells with the uncoated beads for comparison.

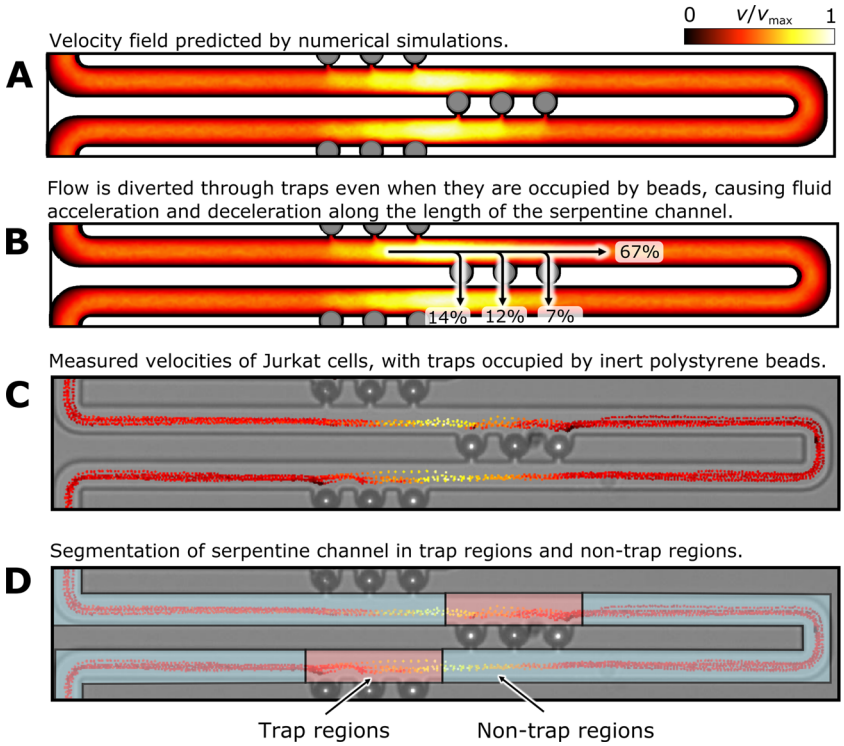

FIG. 2. Comparison between experimental and measured flow through the hydrodynamic trap array. (a) 3D COMSOL simulation of flow through the device, with all traps occupied by 15 μm diameter beads. (b) The fluid velocity is expected to increase near the center of each turn of the serpentine channel due to flow past trapped beads in the previous lane. (c) Measured velocities of Jurkat cells flowing past inert polystyrene beads. (d) The "speed ratio" is defined as the ratio of a cell's median speed in trap regions to its median speed in non-trap regions.

As expected, for the device loaded with antibody-coated beads, most cells entering the channel immediately bound to the beads and remained attached for the duration of the measurement. Of the Jurkat cells entering the channel, 88% (23 out of 26 cells) became permanently attached to the antibody-coated beads. In contrast, only 17% of the cells (2 out of 12 cells) became permanently attached to inert polystyrene beads in the corresponding negative control measurement. The cells that seemingly attached to the inert, unconjugated beads were likely not attached to the beads themselves, but were captured in the traps along with the beads due to the residual flow across the beads and into the next lane.

These results demonstrate that antibody-antigen interactions can be detected using the trap array platform. However, due to the permanent attachment of cells to beads, only the binary metric of attachment, rather than speed changes, could be used to quantify the strength of this type of interaction.

2. TCR–pMHC interaction

Next, we asked whether this approach could detect specific TCR–pMHC interactions in primary $CD8^+$ T cells from OT-1 TCR transgenic mice, which recognize the peptide SIINFEKL presented by $H\text{-}2K^b$ MHC class I. We loaded the trap array with $H\text{-}2K^b$:SIINFEKL-coated beads and then flowed the OT-1 $CD8^+$ T cells through the channel. As a negative control, we emptied the trap array, loaded the traps with Bovine serum albumin (BSA)-coated beads, and flowed more OT-1 $CD8^+$ T cells through the channel.

T cell speed ratios (trap speed/non-trap speed) were reduced significantly when the T cells interacted with $H\text{-}2K^b$:SIINFEKL-conjugated beads compared to when they interacted with BSA-conjugated beads [$p < 2 \times 10^{-6}$, Mann-Whitney; Fig. 3(a)]. Although the absolute flow rate varied over the course of the measurement, speed ratios remained approximately constant

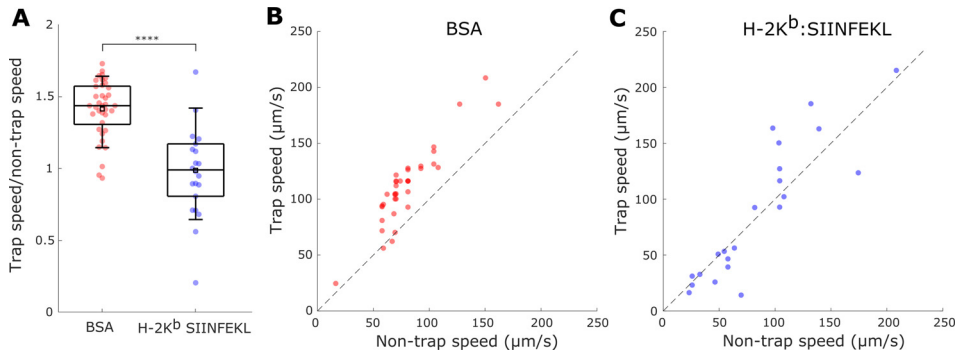

FIG. 3. (a) Speed ratios of OT-1 CD8$^+$ T cells interacting with beads coated with BSA or H-2K^b SIINFEKL. Each point represents a single cell. Specific TCR–pMHC interactions significantly ($p < 2 \times 10^{-6}$, Mann-Whitney) reduced the speeds of OT-1 CD8$^+$ T cells flowing through the device ($n = 37$ cells), compared with OT-1 CD8$^+$ T cells interacting with BSA-coated beads ($n = 21$ cells). (b) and (c) Median speeds of each cell when in trap regions versus non-trap regions. Cells had similar speed ratios even though their trap- and non-trap speeds varied.

[Figs. 3(b) and 3(c)]. As expected, cell speed in trapping region was faster than in the non-trap region (i.e., speed ratio greater than 1) due to flow past trapped beads in the previous lane, but after interaction with H-2K^b:SIINFEKL, the speed ratio was reduced. We observed the same response in CD8$^+$ T cells isolated from a second OT-1 TCR transgenic mouse; that is, in this independent biological replicate, the H-2K^b:SIINFEKL-conjugated beads significantly reduced cell speed ratios compared with BSA-conjugated control beads ($p < 0.01$; $n = 21$ and $n = 20$ cells for the H-2K^b:SIINFEKL- and BSA-conjugated beads, respectively; data not shown).

III. DISCUSSION AND CONCLUSION

These results suggest that the cell speed-based affinity measurement modality is capable of detecting specific TCR–pMHC interactions. As implemented here with a single serpentine channel, the system achieves a throughput of 3–5 cells per minute with 24–30 cell-bead interactions observed per cell. A key advantage of this approach is that it is scalable; while these prototype devices contained just a single serpentine channel, throughput could be increased further by combining multiple in parallel on the same device and imaging them simultaneously. Depending on the application, the total throughput (i.e., experimental conditions measured per unit time) may be limited by the time required for cell isolation and sample preparation, rather than the time required to run the assay. In these applications, throughput would benefit more from advances in sample preparation, such as novel microfluidic techniques for high-throughput cell sorting.[20]

There are several practical challenges associated with the device operation that should be considered in future efforts to scale up. For example, the range of affinities that can be measured by a particular device is constrained by the device geometry and flow rate. Although the flow rate through the channel can be adjusted so that the viscous force is comparable to the interaction strength, F_{int}, in practice this requires a prior estimate of the interaction strength, which is not always suitable for mixed populations of cells where affinities and interaction forces could vary greatly. In the case of high-affinity interactions, the result is that cells become permanently attached to beads and obstruct the serpentine channel until cleared. In the future, it is possible that this assay could be modified to measure high-affinity cell-bead interactions by first forming permanent cell-bead attachments, then gradually increasing the hydrodynamic shear rate until the TCR:pMHC bonds break, analogous to a novel shear-enhanced protein detection method described previously.[21] Additionally, in future designs, a shorter serpentine channel with fewer turns could help to assist in clearing the channel, enabling measurement of more cells per unit time, at the expense of observing fewer cell-bead interactions per cell.

Looking forward, this measurement approach is potentially compatible with a variety of cell types and model systems, conceivably including loading the traps with primary antigen-presenting cells rather than synthetic antigen-presenting beads. In some clinical applications,

loading primary patient antigen-presenting cells into the hydrodynamic traps could enable the study of primary T cells even when patient HLA (human leukocyte antigen) haplotype may be unknown.

A further extension of this work would be to collect single T cells off-chip after measurement to link affinity with downstream single-cell analysis, as demonstrated previously.[22,23] For example, single-cell genome sequencing could be used to identify T cells in mixed populations to provide context for the observed heterogeneity in affinity measurements. Alternatively, single-cell transcriptome sequencing could be used to explore the early transcriptional events following TCR engagement by varying combinations of pMHC and co-receptors. The versatility of the microfluidic trap array platform suggests that it may be broadly useful in T cell immunology.

IV. EXPERIMENTAL

A. Device fabrication

The trap arrays were fabricated in 6-in. silicon-on-insulator (SOI) wafers. The channels and traps were etched using deep reactive ion etching into the SOI device layer. Next, the wafer was anodically bonded to a Pyrex lid to enable optical access to the channels for microscope imaging. Fluidic access ports were then etched through the wafer from the backside.

B. System assembly

Pressure-driven flow through the device is controlled using a combination of electronic pressure regulators (Proportion Air) and solenoid valves (SMC). Fluidic connections to the device are made using perfluoroelastomer O-rings, which are clamped to the device between an aluminum or acrylic face plate and a polytetrafluoroethylene (PTFE) gasket to form a seal. The device is imaged using an upright microscope (Nikon) with a 10× or 20× objective (Nikon, CFI Plan Fluor), and video is recorded at 18–21 frames per second using a Hamamatsu Orca-ER CCD or Edmund Optics 1312M camera. Temperature is maintained at 37 °C using a recirculating water bath (Thermo Scientific).

C. Device operation

In preparation for each measurement, air bubbles are flushed out of the trap array by priming with ethanol, and then with deionized water. To passivate the surface of the device and reduce nonspecific protein adsorption, the channels are then coated with 1 mg ml^{-1} PLL-*g*-PEG (Surface Technology) by incubating for 30 min. The device is rinsed again with water and primed with Hank's balanced salt solution (HBSS; Thermo Fisher). All priming solutions are 0.2 μm-filtered prior to introduction into the device.

Beads are then loaded into the device at a concentration of approximately 5×10^4 beads ml^{-1}. The device is rinsed again with HBSS to remove any excess beads. Then, a cell suspension in HBSS is loaded into the device at an approximate concentration of 2×10^6 cells ml^{-1}. After cells are loaded into the device, flow rates are lowered and maintained at a constant value (0.3–0.6 psi applied pressure) throughout the measurement; typically, cells flow through the serpentine channel with speeds of order 10–50 $\mu m\ s^{-1}$.

After each experiment, the device is cleaned using a 10% bleach solution and rinsed with deionized water. The device can then be re-passivated and used for the next experiment.

D. Data analysis

Analysis of the videos is performed using MATLAB to track the trajectories and speeds of individual cells as they transit the serpentine channel. First, positions of the cells in each frame are identified using the circular Hough transform. The list of cell positions is grouped into trajectories corresponding to single cells using the existing particle tracking methods.[24] Then, for each cell, the instantaneous velocity in each frame is computed using a centered finite difference approximation.

E. Cell culture

Jurkat cells (ATCC TIB-152) were cultured in RPMI medium (Thermo Fisher) supplemented with 10% fetal bovine serum (FBS), 25 mM HEPES, and 1% antibiotic-antimycotic (Gibco).

$CD8^+$ T cells were isolated from the spleens of OT-1 mice via negative magnetic selection (Miltenyi, $CD8^+$ T Cell Isolation Kit). T cells were activated by plating them at a concentration of 2×10^6 cells ml^{-1} in a high-bind 96 well plate coated with 5 $\mu g\,ml^{-1}$ anti-mouse CD3 antibody (clone: 145–2C11, BioLegend catalog number 100314) while having 2 $\mu g\,ml^{-1}$ anti-mouse CD28 (clone: 37.51, BioLegend catalog number 102112) and 100 U ml^{-1} mouse IL-2 (Miltenyi) in solution. Cells were cultured for 48 h, then collected, centrifuged, and resuspended in HBSS for measurement. Alternatively, in some cases $CD8^+$ T cells were activated by culturing with 10 μM SIINFEKL peptide (Sigma-Aldrich) and 100 U ml^{-1} mouse IL-2 for seven days. Cells were cultured in RPMI supplemented with 10% FBS, 25 mM HEPES, 50 μM 2-mercaptoethanol (Gibco), and 1% antibiotic-antimycotic (Gibco).

F. Streptavidin bead functionalization

Bovine serum albumin (BSA)- and SIINFEKL-conjugated beads were prepared using 15 μm diameter streptavidin-coated polystyrene beads (Bangs Laboratories). Biotinylated BSA (Vector Laboratories) or biotinylated H-$2K^b$:SIINFEKL (MBL International) was conjugated to the beads by incubating 1×10^6 beads ml^{-1} with 10 $\mu g\,ml^{-1}$ protein in phosphate-buffered saline (PBS) for 3 h at room temperature. Beads were then rinsed twice with PBS and stored at 4 °C. Conjugation of H-$2K^b$:SIINFEKL was confirmed using flow cytometry by staining the beads with APC anti-mouse H-$2K^b$:SIINFEKL (BioLegend). Based on the reported binding capacity for the streptavidin beads, the streptavidin binding site density is approximately $9 \times 10^4\,\mu m^{-2}$; however, due to the ~2.4 nm radius of the conjugated proteins, we expect binding to be limited by steric effects to $\sim 4 \times 10^4$ pMHC μm^{-2}, or a total of 4×10^7 pMHC per 15 μm bead. Formation of cell-bead interactions is therefore expected to be limited by TCR availability, since TCRs are typically present at spatial densities of 100–200 μm^{-2}.[25]

G. Carboxylated bead functionalization

Anti-CD3 and anti-CD28 conjugated beads were prepared using 15 μm-diameter carboxylated polystyrene beads (Bangs Laboratories). Anti-human CD3 and anti-human CD28 antibodies (BioLegend) were conjugated to the beads using the PolyLink protein coupling kit (Bangs Laboratories), using 250 μg of each antibody per million beads. After functionalization, the anti-CD3/anti-CD28 beads were resuspended in PBS and stored at 4 °C. While the binding site density is not specified by the bead manufacturer, if the surface is saturated with the ~3.5 nm radius antibodies we expect $\sim 2 \times 10^7$ Ab μm^{-2}; that is, formation of cell-bead interactions is still limited by availability of CD3 and CD28, which we assumed are present on the cell membrane at spatial densities similar to those of T cell receptors (100–200 μm^{-2}).[25]

H. Numerical simulations

We used a 3D finite element solver (COMSOL) to investigate flow through the device with various bead loading conditions. A 3D model of the microfluidic channel was meshed using tetrahedral elements, and the 3D steady Navier-Stokes equations were solved with constant-pressure boundary conditions at the inlet and outlet of the channel. The 15 μm beads were modeled as rigid spheres fixed at the midplane of the channel.

ACKNOWLEDGMENTS

This work was supported by U54 CA143874 and R21 AI110787 from the National Institutes of Health. We thank Gregory Szeto and Sudha Kumari for insightful and informative discussion, as well as access to materials. We also thank Michael Birnbaum for thoughtful discussion and feedback on the manuscript. This work was carried out in part through the use of MIT's

Microsystems Technology Laboratories. M.A.S. acknowledges support from a National Science Foundation GRFP fellowship.

[1]J. D. Stone, A. S. Chervin, and D. M. Kranz, Immunology **126**, 165–176 (2009).
[2]P. O. Gannon, S. Wieckowski, M. Hebeisen, M. Allard, E. Speiser, N. Rufer, M. Allard, D. E. Speiser, and N. Rufer, J. Immunol. **195**, 356–366 (2015).
[3]S. Zhang, P. Parker, K. Ma, C. He, Q. Shi, Z. Cui, C. M. Williams, B. S. Wendel, A. I. Meriwether, M. A. Salazar, and N. Jiang, Sci. Transl. Med. **8**, 341ra77 (2016).
[4]Z. Ma, D. E. Discher, and T. H. Finkel, Front. Immunol. **3**, 1–3 (2012).
[5]K. M. Armstrong, F. K. Insaidoo, and B. M. Baker, J. Mol. Recognit. **21**, 275–287 (2008).
[6]J. Huang, V. I. Zarnitsyna, B. Liu, L. J. Edwards, N. Jiang, B. D. Evavold, and C. Zhu, Nature **464**, 932–936 (2010).
[7]D. K. Das, Y. Feng, R. J. Mallis, X. Li, D. B. Keskin, and R. E. Hussey, PNAS **112**, 1517–1522 (2015).
[8]C. Gourier, A. Jegou, J. Husson, and F. Pincet, Cell. Mol. Bioeng. **1**, 263–275 (2008).
[9]B. Liu, W. Chen, B. D. Evavold, and C. Zhu, Cell **157**, 357–368 (2014).
[10]H. J. Zeh, D. Perry-Lalley, M. E. Dudley, S. A. Rosenberg, and J. C. Yang, J. Immunol. **162**, 989–994 (1999).
[11]M. Nauerth, B. Weißbrich, R. Knall, T. Franz, G. Dössinger, J. Bet, P. J. Paszkiewicz, L. Pfeifer, M. Bunse, W. Uckert, R. Holtappels, D. Gillert-marien, M. Neuenhahn, A. Krackhardt, and M. J. Reddehase, Sci. Transl. Med. **5**, 192ra87 (2013).
[12]L. A. Johnson, R. A. Morgan, M. E. Dudley, L. Cassard, J. C. Yang, M. S. Hughes, U. S. Kammula, R. E. Royal, R. M. Sherry, J. R. Wunderlich, C. R. Lee, N. P. Restifo, S. L. Schwarz, A. P. Cogdill, R. J. Bishop, H. Kim, C. C. Brewer, S. F. Rudy, C. Vanwaes *et al*., Blood **114**, 535–546 (2009).
[13]M. Hebeisen, M. Allard, P. O. Gannon, J. Schmidt, D. E. Speiser, and N. Rufer, Front. Immunol. **6**, 1–18 (2015).
[14]U. Schneider, H. Schwenk, and G. Bornkamm, Int. J. Cancer **19**, 621–626 (1977).
[15]S. R. Clarke, M. Barnden, C. Kurts, F. R. Carbone, J. F. Miller, and W. R. Heath, Immunol. Cell Biol. **78**, 110–117 (2000).
[16]M. Makhoul, P. Beltrame, and M. Joelson, Int. J. Mech. **9**, 260–271 (2015).
[17]T. A. Sulchek, R. W. Friddle, K. Langry, E. Y. Lau, H. Albrecht, T. V. Ratto, S. J. Denardo, M. E. Colvin, and A. Noy, Proc. Natl. Acad. Sci. U.S.A. **102**, 16638 (2005).
[18]W.-H. Tan and S. Takeuchi, Proc. Natl. Acad. Sci. U.S.A. **104**, 1146–1151 (2007).
[19]D. Jin, B. Deng, J. X. Li, W. Cai, L. Tu, J. Chen, Q. Wu, and W. H. Wang, Biomicrofluidics **9**, 014101 (2015).
[20]S. A. Faraghat, K. F. Hoettges, M. K. Steinbach, D. R. Van Der Veen, and W. J. Brackenbury, Proc. Natl. Acad. Sci. U.S.A. **114**, 4591–4596 (2017).
[21]D. Li, C. Wang, G. Sun, S. Senapati, and H. Chang, Biosens. Bioelectron. **97**, 143–149 (2017).
[22]R. J. Kimmerling, G. L. Szeto, J. W. Li, A. S. Genshaft, S. W. Kazer, K. R. Payer, J. D. R. Borrajo, P. C. Blainey, D. J. Irvine, A. K. Shalek, and S. R. Manalis, Nat. Commun. **7**, 10220 (2016).
[23]J. S. Bagnall, S. Byun, and D. T. Miyamoto, Integr. Biol. **8**, 654–664 (2016).
[24]I. Hosein, MATLAB File Exchange, 2013.
[25]N. Labrecque, L. S. Whitfield, R. Obst, C. Waltzinger, C. Benoist, D. Mathis, and L. Fries, Immunity **15**, 71–82 (2001).